Title

Stream-dependent development of higher visual cortical areas.

Journal

Nature neuroscience, 20(2)

ISSN

1097-6256

Authors

Smith, Ikuko T
Townsend, Leah B
Huh, Ruth
et al.

Publication Date

2017-02-01

DOI

10.1038/nn.4469

Peer reviewed

HHS Public Access

Author manuscript

Nat Neurosci. Author manuscript; available in PMC 2017 July 09.

Published in final edited form as:

Nat Neurosci. 2017 February ; 20(2): 200–208. doi:10.1038/nn.4469.

Stream-dependent development of higher visual cortical areas

Ikuko T. Smith[1,2], **Leah B. Townsend**[3], **Ruth Huh**[6], **Hongtu Zhu**[6], and **Spencer L. Smith**[1,4,5]

[1]Neuroscience Center, University of North Carolina School of Medicine, Chapel Hill, NC 27599

[2]Department of Pharmacology, University of North Carolina School of Medicine, Chapel Hill, NC 27599

[3]Neurobiology Curriculum, University of North Carolina School of Medicine, Chapel Hill, NC 27599

[4]Department of Cell Biology and Physiology, University of North Carolina School of Medicine, Chapel Hill, NC 27599

[5]Carolina Institute for Developmental Disabilities, University of North Carolina School of Medicine, Chapel Hill, NC 27599

[6]Department of Biostatistics, and Biomedical Research Imaging Center, University of North Carolina School of Medicine, Chapel Hill, NC 27599

Abstract

Multiple cortical areas contribute to visual processing in mice. However, the functional organization and development of higher visual areas are unclear. Here, we used intrinsic signal optical imaging and 2-photon calcium imaging to map visual responses in adult and developing mice. We found that visually driven activity was well-correlated among higher visual areas within two distinct subnetworks resembling the dorsal and ventral visual streams. Visual response magnitude in dorsal stream areas slowly increased over the first two weeks of visual experience. By contrast, ventral stream areas exhibited strong responses shortly after eye opening. Neurons in a dorsal stream area showed little change in their tuning sharpness to oriented gratings while those in a ventral stream area increased stimulus selectivity and expanded their receptive fields significantly. Together, these findings provide a functional basis for grouping subnetworks of mouse visual areas and revealed stream differences in the development of receptive field properties.

Corresponding authors: I.T.S. (ikukots@unc.edu) and S.L.S. (slab@unc.edu). Contact for editorial correspondence: Spencer L. Smith, slab@unc.edu, Phone: 1-919-966-2349, CB#7545, 111 Mason Farm Road, Chapel Hill, NC 27599-7545, USA.

AUTHOR CONTRIBUTIONS

I.T.S. and S.L.S. conceived and designed the experiments. I.T.S. and L.B.T. performed the intrinsic signal optical imaging experiments and analyzed data. I.T.S. and S.L.S. performed the calcium imaging experiments and analyzed data. R.H. and H.Z. performed some of the statistical analysis. I.T.S. and S.L.S. interpreted the data and wrote the paper.

COMPETING FINANCIAL INTERESTS

The authors declare no competing financial interests.

INTRODUCTION

Mammalian visual cortex is comprised of a primary visual cortex (V1; also known as striate cortex) and several higher visual areas (HVAs, or extrastriate cortex). Together, V1 and HVAs form an intricate and reciprocally connected network[1–6]. Lesion studies in primates[7,8] have revealed distinct functions for two parallel visual processing pathways: the ventral and dorsal streams. The ventral stream is crucial for form vision and object recognition, while the dorsal stream is important for perception of motion in visual stimuli[9,10].

Recent anatomical studies in mouse cortex revealed two subnetworks of HVAs that resemble the ventral and dorsal streams seen in primates[2,3,11]. Of the areas immediately surrounding V1, two lateral areas, lateralmedial (LM) and laterointermediate (LI), have been anatomically identified as nodes of a ventral stream pathway, and posteromedial (PM), anteromedial (AM), anterior (A), rostrolateral (RL) and anterolateral (AL) areas as nodes of a dorsal stream pathway[3]. Projections among V1 and HVAs exhibit specific expression patterns of pre- and postsynaptic receptors such as metabotropic glutamate activation[12–14]. Moreover, projections from HVAs to V1 form distinct network structures that manifest in patches around M2 muscarinic acetylcholine receptor-rich regions[15]. These findings are indicative of distinct synaptic drive and modulation among HVAs that likely convey unique functional properties[16,17].

Attempts to understand the functional organization of HVAs, on the other hand, have produced conflicting results. The tuning properties of HVAs are area-specific, varying in temporal and spatial frequency preferences[18,19], and axonal boutons originating from V1, an area with a wide range of receptive field properties, are specifically tuned to the preferred properties of the postsynaptic target HVAs in which they terminate[20]. In these studies, dorsal stream HVAs exhibited strong selectivities for direction and orientation[18,19,21], in line with the suggested roles of dorsal stream in perceiving motion. In contrast, another study examining HVA responses to plaid motion stimuli suggested that LM, an anatomically described ventral stream HVA[3], is functionally placed in the dorsal stream capable of responding to integrated global motion[22]. Thus, a consensus on functional delineations between putative dorsal and ventral streams in mice has been elusive. Those that work together may develop together. To understand the selective structuring of the mouse visual circuitry, we sought to determine how the HVAs functionally develop during the postnatal period immediately after eye-opening.

Here, we used intrinsic signal optical imaging (ISOI) and 2-photon calcium (2p Ca^{2+}) imaging to investigate correlated activity among V1 and HVAs, and to determine the developmental time course of visual responses of HVAs in mice. We found that HVAs in mice form two subnetworks, which match anatomically identified putative analogs of the dorsal and ventral streams in primates. The two subnetworks are functionally distinct in their activity patterns, developmental time courses, and single-cell receptive field properties. Post-eye opening, visual response maturation of dorsal stream HVAs was noticeably slower than that of the ventral stream HVAs, and was vulnerable to a lack of visual experience. Subsequent re-exposure to light failed to induce a full recovery of dorsal stream HVAs. Neurons in ventral stream area, on the other hand, sharpened their orientation tuning and

increased the receptive field size during development despite the modest change in their overall response strength. These findings, to our knowledge, provide for the first time a functional basis for the classification of the two HVA networks, dorsal and ventral streams in mice.

RESULTS

Mapping visual areas using intrinsic signal optical imaging

ISOI was used to measure neural activity in V1 and HVAs. Mice viewed a stimulus monitor placed obliquely to cover 5° to 115° of the contralateral visual hemifield. Stimuli that appeared at the center of the monitor were thus positioned at 60° in the animals' lateral visual field. Visual stimuli positioned at such an angle activate both medial and lateral HVAs equally well in adult mice[19,23]. Retinotopic maps of visual cortex were obtained using a high contrast bar drifting in elevation or azimuth, and allowed reliable identification of V1 and six HVAs, PM, AM, RL, AL, LM and LI (Fig. 1a–d). The borders of area A could be inferred after mapping adjacent HVAs and V1, however, we did not observe reliable visually evoked activation in area A (ref. [18]). The topographical representation of the visual hemifield observed in V1 was also preserved within the HVAs, in either reversed order (sharing a meridian with a neighboring area) or with a twist in the orientation (e.g. compare azimuth retinotopy in PM and V1). Thus, the two orthogonal retinotopic maps, elevation and azimuth (Fig. 1c,d), together revealed the precise locations of horizontal and vertical meridians, which defined the borders among V1 and HVAs[1,18,24]. Regions of interest (ROIs) for quantitative analysis of evoked activity in V1 and HVAs were drawn using these meridians as landmarks. The only exception was the border between AM and PM. Although there was a reliable meridian in adult mice, the delineation between the two areas was not reliable in developing pups. Therefore, to ensure reliable and conservative analysis across all ages studied, these two areas were grouped together as AM/PM for quantification. In a subset of animals, a small square aperture (10° × 10°) with drifting gratings of rapidly changing orientation were presented which evoked discernable visually responsive areas in individual HVAs (Fig. 1e,f). These maps confirmed the reliability of the ROIs drawn on retinotopic maps generated using drifting single bar stimuli. The retinotopic maps were superior to the maps generated by small aperture gratings for mapping HVAs as the retinotopic maps revealed each entire area rather than a small portion.

After mapping HVAs with drifting bars, we measured evoked activity levels in V1 and HVAs using the magnitude of the intrinsic signal in response to square wave gratings and random dot kinematogram visual stimuli (see **Methods** and Supplementary Fig.1). Each stimulus was stationary for six seconds and in motion for two seconds comprising a stimulus period of eight seconds that repeated for 50 cycles. To first examine the relative functional properties among V1 and HVAs in mature circuitry, we imaged visual responses in adult mice (≥ P40).

Response correlations among HVAs

Because we simultaneously imaged V1 and HVAs, we were able to reduce each map to a six dimensional vector, with each element representing the average activation level in a cortical

area. We used these vectors to examine correlations in activation among the areas in adult mice (P40 – P65, $n = 22$). Response magnitudes in most HVAs were well correlated (Pearson's $R > 0.5$) with activity in V1 (Supplementary Fig. 2a,b). This is expected for two reasons. First, V1 provides strong input to HVAs, with the remaining input emerging from other cortical areas[3], thalamic nuclei, and other brain structures. Second, general response levels can be affected globally with anesthetic depth[25]. In fact, while raw response magnitude measurements were heavily affected by the depth of anesthesia, values for individual HVAs normalized to the same animal's V1 measurement were noticeably resistant to the changes in anesthesia level (Supplementary Fig. 3).

Overall, correlation coefficients were higher for adjacent cortical areas (e.g., RL and AL: Pearson's $R = 0.94$ for gratings, 0.84 for kinematograms; $P < 0.0001$ for both; Supplementary Fig. 2a,b), and lower for areas that do not share a border (e.g., V1 and LI: Pearson's $R = 0.55$ for gratings, 0.42 for kinematograms; $P = 0.0087$, $P = 0.0048$, respectively; Supplementary Fig. 2a,b). An exception to this general trend is the high correlation between AM/PM and AL (Pearson's $R = 0.94$ for gratings, 0.82 for kinematograms; $P < 0.0001$ for both; Supplementary Fig. 2a,b), which are on opposite sides of V1. This exception is consistent with AL and AM/PM being components of the same processing network, analogous to the dorsal stream, as suggested by previous anatomical studies[2,3,11].

Next, we investigated the correlations among the HVAs. For this analysis, raw response magnitudes from the intrinsic signal maps were normalized to the average response magnitude of V1 within each map. This provides a control for general levels of cortical response per mouse (Supplementary Fig. 3), and correlation coefficients computed after this normalization reflect correlations among HVAs themselves. Areas AL, RL, and AM/PM exhibited high correlations among each other in response magnitudes across maps evoked by both gratings and kinematograms. Similarly, areas LM and LI were well correlated in their response magnitudes. The clustering of the two streams remained strong even when correlations varied between stimulus types (Fig. 1g,h; Supplementary Table 1). This suggests that LM and LI are components of one subnetwork while AL, RL, and AM/PM are components of another. Principal component analyses (PCA) on the response magnitudes also supported the grouping of HVAs into anatomically identified dorsal and ventral areas[3] (Fig. 1i,j). Thus, by measuring response magnitudes to visual stimuli in V1 and six HVAs simultaneously, we detected correlations that provide functional evidence to support the grouping of HVAs into anatomically identified[2,3] dorsal and ventral streams. Accordingly, we proceeded to group the AM/PM, RL and AL as dorsal, and LM and LI as ventral stream subnetworks for further comparative analyses between the two streams.

Early and late-developing HVAs: ventral and dorsal stream pathways and their experience-dependence

We next examined the functional development of HVAs in juvenile mice. Visually evoked activity was measured in developing pups immediately following eye opening at P13 to P36 (Fig. 2). In pups of ages P13 – P18, ISOI was performed transcranially. In these instances, the skull was rendered optically transparent by immersing in physiological saline. For pups

of ages from P20 – P36, the skull overlaying the visual cortex was removed to install a cranial window for chronic intrinsic imaging[26]. This approach prevented the growing thickness of the skull from interfering with optical imaging[27] (Supplementary Fig. 4), and allowed for repeated imaging once every four days for over two weeks. Imaging of visually evoked cortical responses was possible shortly after eye opening[28] (Fig. 2a,b). Grating patches evoked cortical activity that revealed a prominent dichotomy in the developmental trajectory of the two subnetworks. Ventral stream HVAs were responsive shortly after eye opening and quickly matured within the first few days of visual experience. By contrast, dorsal stream HVAs were only weakly responsive in immature pups and slowly developed over the next two weeks (ANOVA: dorsal stream, $P < 0.0001$; ventral stream, $P = 0.4186$; Tukey-Kramer HSD: dorsal stream P13 – 18, $P < 0.0001$; P20, $P = 0.0002$; P24, $P = 0.036$; P28, $P = 0.90$; P32, $P = 0.037$; Fig. 2b,c). The differential developmental time courses were also observed in individual HVAs among which AM/PM, RL, and AL took two weeks after eye opening to develop their response amplitude whereas LM and LI showed strong response as early as a couple of days after eye opening (Supplemental Fig. 5). The observed differential functional development was not stimulus-type specific. As seen with gratings, responses to kinematograms developed more slowly in dorsal stream HVAs compared to the ventral stream HVAs (ANOVA: dorsal stream, $P = 0.0007$; ventral stream, $P = 0.0016$; Tukey-Kramer HSD: dorsal stream, P15/16, $P = 0.0008$; P17/18, $P = 0.0033$; P20, $P = 0.0061$; ventral stream, P17/18, $P = 0.0013$; Fig. 2d).

Delayed development of dorsal stream HVAs suggested that these areas require visual experience post eye opening for normal circuit refinement. To test this idea, we dark-reared (DR) mice from E14 through P40 (Fig. 2e) and measured cortical visual responses to grating stimuli using ISOI. Indeed, P40 mice raised in complete darkness showed significantly weaker responses to the visual stimulus in dorsal stream areas (ANOVA: $P = 0.028$; $n = 9$ DR mice, $n = 13$ P40 control mice; Fig. 2f, h). Notably, the response in ventral stream HVAs only shows a slight but non-significant decrease compared to those in mice reared normally (ANOVA: $P = 0.16$; Fig. 2h), suggesting that dorsal stream areas require visual experience for proper functional development while ventral stream areas are more resilient to deprivation. Analysis of individual HVAs revealed that visual responses in areas AM/PM and AL are significantly lower in DR mice compared to control P40 mice ($P = 0.0071$, $P = 0.0351$, respectively), and these effects are greater than DR effects observed in ventral stream area LM ($P = 0.0110$, $P = 0.0319$, respectively; see **Methods** for statistical analysis). Moreover, in mice reared in darkness to P40 and then reared normally for 25 days to P65, dorsal stream HVAs remained less responsive (ANOVA: $P = 0.0045$), while normal visual responses were observed in ventral stream HVAs (ANOVA: $P = 0.39$; $n = 9$ recovery mice, $n = 9$ P65 control mice; Fig. 2e, g, h). These results indicate that the experience-dependent development of dorsal stream HVAs is restricted to an early time window prior to P40.

Visual responses at individual neuron resolution

To understand the cellular underpinnings of the quantitative data from ISOI, we also performed 2p Ca^{2+} imaging experiments. We first directly compared the relative responsiveness from intrinsic signal maps and 2p $Ca2^{+}$ imaging at the single cell level

within the same adult mice that expressed virally-transduced genetically encoded Ca^{2+} indicator, GCaMP6s (Fig. 3).

The data from ISOI were quantified as an average intrinsic signal magnitude per cortical area. By contrast, the data from 2p Ca^{2+} imaging were action potential associated calcium transients for individual neurons (Fig. 3a,b). To compare these very different data sets, ratios of responsiveness between cortical areas were used. For intrinsic signal maps, the responsiveness was simply measured as a ratio of average intrinsic signals between two cortical areas. For 2p Ca^{2+} imaging data, the fraction of cells that responded on a given stimulus presentation (averaged over 50 cycles) was computed. Measurements from two different cortical areas were then used to construct a ratio. The calculated ratios for Ca^{2+} imaging and intrinsic signal magnitude for the same cortical areas were compared in the same mouse in response to the same visual stimulus. The results showed a high correlation between intrinsic and calcium signals ($R = 0.92$, $P = 0.027$; $n = 5$; Fig. 3c). This is consistent with previous work demonstrating that hemodynamic intrinsic signals faithfully reflect underlying neuronal activity in the mouse[29–31].

Next, we sought to compare the development of a dorsal stream area to that of a ventral stream area on the cellular level. To this end, we measured fundamental receptive field properties in PM (dorsal stream) and LM (ventral stream) in GCaMP6s-expressing transgenic mice at P20 and P36.

Developmental changes in responses to drifting gratings

We first examined the cellular response to oriented gratings, the stimuli used for ISOI. To examine cellular responses in further detail and detect area-specific response property development, we used 12 different directions and two spatial frequencies: 0.04 cycles/degree (low spatial frequency, LSF: matched to gratings used for ISOI), and 0.32 cycles/degree (high spatial frequency, HSF). In accordance with the ISOI results, response magnitude in PM neurons significantly increased between P20 and P36 to LSF gratings of all directions while LM neurons showed significant but more modest increase (Fig. 4a,b; P20–P36 increase in LM neurons = 1.3 ± 0.053; in PM neurons = 1.7 ± 0.082; $P < 0.0001$, rank-sum test for both; increase in PM > increase in LM, $P < 0.0001$, rank sum test; $n = 266$ LM neurons at P20, 442 at P36, 341 PM neurons at P20, 329 at P36). Moreover, PM response strengthened significantly more for HSF than LSF gratings ($P < 0.0001$, rank-sum test), whereas LM response modestly increased to a similar extent for both HSF and LSF gratings (Fig. 4a–d; $P < 0.0001$, rank-sum test; HSF-LSF difference > in PM than LM, $P < 0.0001$, rank-sum test).

Developmental changes in orientation tuning

Next we examined the development of orientation selectivity in V1, PM and LM neurons (for 0.04 cycles/deg, P20: $n = 90$ V1 cells, 50 LM cells, and 95 PM cells; P36: $n = 286$ V1 cells, 178 LM cells, and 47 PM cells; for 0.32 cycles/deg P20: $n=127$ V1 cells, 44 LM cells, and 56 PM cells, P36: $n = 191$ V1 cells, 105 LM cells, and 39 PM cells; Fig. 5). The orientation selectivity index (OSI) significantly increased for all three areas for stimulation with LSF gratings (Fig. 5b, $P < 0.0001$ for all three areas). Our finding for V1 is consistent

with a prior report[32]. When HSF gratings were used (Fig. 5c), OSI measurements showed a significant increase for LM neurons ($P = 0.0001$), a slight increase for PM neurons ($P = 0.03$), and a small decrease for V1 neurons ($P = 0.04$). The modest developmental increase in OSI of PM neurons in response to HSF gratings should be considered in the context of already high OSI values for HSF at P20 which were comparable to that of P36 PM neurons in response to LSF gratings (mean ± SEM; PM, P20, HSF: 0.64 ± 0.18; PM, P36, LSF: 0.63 ± 0.19; $P = 0.98$, rank-sum test). Direction selectivity (as measured by the direction selectivity index, DSI) for both LSF and HSF gratings remained unchanged in LM or PM while V1 neurons showed a decrease in DSI for LSF gratings ($P = 0.0002$; Supplementary Fig. 6).

Developmental changes in receptive field (RF) maps

RF mapping can provide insights into basic wiring principles of visual circuitry[33,34]. We mapped the ON and OFF RF subregions of V1, PM, and LM neurons in P20 and P36 mice, using sparse noise stimuli and reverse correlation, as previously described[33] (Fig. 6). Neurons in all three areas exhibited ON or OFF RF subregions (at P20: n = 19, 15, 14 ON subregions, and n = 41, 45, 12 OFF subregions for V1, LM, and PM, respectively; at P36: n = 23, 44, 7 ON subregions, and n = 48, 18, 10 OFF subregions for V1, LM, and PM, respectively). Structural measurements revealed that the RF subregion size of LM neurons was significantly larger in P36 mice compared to P20 mice, while those of V1 and PM neurons were indistinguishable (for LM, V1, and PM, respectively: $P < 0.0001$, $P = 0.82$, $P = 0.75$, ON and OFF RF subregions pooled). The LM RFs were larger along both the long and short axes, thus preserving the aspect ratio of the RFs similar between the ages (Fig. 6a–d; Supplementary Fig. 7). Despite the spatial changes observed in LM, the RF subregions exhibited similar temporal characteristics. Specifically, the peak of the RF subregion strength in the reverse correlation analysis (the time difference between stimulus presentation and maximal influence on neuronal activity) was similar across areas, ages, and subregion signs (Supplementary Fig. 8). Finally, consistent with a prior report, we observed RF subregions in V1 that were precisely shared between different neurons[33]. Similarly, shared RF subregions were also observed in areas LM and PM (Fig. 6e,f).

DISCUSSION

One of the hallmarks of neocortex is the parcelization of parenchymal areas that act as functional units[1,5]. In this study, we measured responses in V1 and HVAs in developing mice. To our knowledge, this study provides the first characterization of the functional developmental trajectories of HVAs. We found functional correlations, development patterns, and sensitivities to dark rearing that distinguished putative dorsal stream HVAs (AM, PM, RL and AL) from the ventral stream HVAs (LM and LI). The delayed development of dorsal stream HVAs was also reflected in the development of receptive field properties on a single-cell level quantified using 2p calcium imaging. 2p calcium imaging also provided evidence that despite its relatively stable response strength, ventral stream circuitry continues to expand and integrate more inputs as reflected by the increase in its receptive field size during development. Together, these data indicate that as in primates, the

two subnetworks of HVAs, dorsal and ventral stream circuitries, can be functionally and developmentally distinct in mice.

Functional and developmental basis for groupings of mouse HVAs

Anatomical projection patterns indicate that mouse HVAs can be grouped into two categories, broadly similar to the dorsal/ventral dichotomy seen in primates[2,3]. In the present study, ISOI enabled simultaneous imaging of functional activity across V1 and multiple HVAs in a single animal. This proved instrumental for detecting correlated activities among certain HVAs, and provided support for the functional grouping of HVAs into two subnetworks. Putative dorsal stream and ventral stream HVAs exhibited stronger correlated variations in the magnitude of their visual responses within their respective subnetworks than with HVAs in the complementary subnetwork. Closer look at the development of response strength by ISOI also highlighted distinct patterns for dorsal and ventral stream. While two ventral stream areas, LM and LI, both exhibited marked visual response immediately after eye-opening, dorsal stream areas, AM/PM, RL and AL showed prominent latency to mature. Notably, AL appeared slightly more developed at eye opening (Supplementary Fig. 5). This is congruent with a previous study that categorized AL to be part of the dorsal stream, but with characteristics somewhat intermediate between dorsal and ventral streams[3]. Differential developmental trajectories for higher visual processing have been observed in humans, where thresholds for global form processing and contour integration, two visual functions attributed to ventral stream pathway, reach adult levels at younger ages than thresholds for global motion processing, a dorsal stream function[35]. Perhaps motion processing circuitry requires a longer duration of visual experience for proper refinement than other types of computational circuitry. This refinement can include both changes in receptive field properties[32,36] and changes in connectivity among V1 and HVAs[20].

Differential development of single-cell level receptive field properties in PM and LM neurons

Calcium imaging in individual HVAs revealed markedly different developmental patterns of visual response properties at the single-cell level in areas PM and LM. Response magnitudes of PM neurons when presented with gratings significantly increased between P20 and P36, mirroring the ISOI results. The observed increase was more prominent for HSF than for LSF, consistent with prior reports of HSF preferences in PM compared to other HVAs[18,19]. However, the OSI of the PM neurons only mildly increased for LSF and remained stable for HSF. The OSI for the PM neurons for HSF gratings was already high at P20; thus, the lack of a further increase in OSI could be due to a ceiling effect. LM neurons, on the other hand, showed only modest increases in the response magnitude for LSF and HSF gratings, again mirroring the ISOI results. In contrast to area PM, however, the OSI of LM neurons sharpened for both spatial frequencies.

From our results emerges a picture for distinct patterns of circuit development in areas PM and LM. Visual responses in PM neurons are relatively late to develop, but as they do so, the responses are already sharply tuned for HSF gratings, possibly because the presynaptic inputs they receive are already highly tuned for HSF[20]. By contrast, the modest increase in

response magnitude of LM neurons, combined with developmental sharpening of tuning for both LSF and HSF gratings, could reflect a combination of relative stability of net synaptic inputs and selective strengthening of inputs that match the tuning preferences of the neuron. Congruent with this idea, the average size of RF subregions of PM neurons remained stable between P20 and P36, while that of LM neurons increased significantly.

Experience-dependent development of HVAs

The distinct patterns of circuit development for PM and LM neurons could be related to different roles visual experience plays in sculpting circuitry in these areas. In particular, the prolonged developmental trajectory of visually evoked responses in dorsal stream HVAs provides a broad time window in which visual experience can influence the maturation of this circuitry. Indeed, through dark rearing experiments, we found that dorsal stream HVAs depend on visual experience for full development of visual responses, whereas ventral stream HVAs were more resistant. This stream-specific vulnerability is reminiscent of the "dorsal vulnerability hypothesis"[37,38]. Based on our findings, such vulnerability may stem from initial targeted innervation by select projections in PM neurons versus continued integration and refinement of inputs in LM neurons.

Our findings offer a scenario in which PM neurons are weakly innervated, strongly inhibited, or biophysically unresponsive to visually driven inputs early in development. Visual responses that subsequently develop post eye-opening are relatively stable in their selectivity, especially for HSF gratings. Thus, developmental refinement of synaptic inputs could occur through strengthening and/or integrating a fixed set of inputs that are tuned upstream of area PM. Indeed, axons projecting from V1 to PM have been shown to be specifically selective for HSF in adult mice[20] (but note that the spatial frequency bias in area PM depends on an intact superior colliculus[39]). Perhaps, only those that are well tuned can reach PM during development rather than a large number of unselective inputs making contacts and later pruned. Because V1 tuning to HSF develops post eye-opening[40], the innervation likely takes place during that time window as well. If deprived of early visual experience with DR, then the strengthening and/or further integration of the inputs are likely prohibited, making PM more vulnerable to DR.

LM neurons, on the other hand, are robustly innervated with visually responsive inputs early, near eye opening (~ P13), before visual experience can have much of an effect. Subsequently, RF subregions expand and tuning sharpens for both LSF and HSF gratings, yet overall response amplitudes change relatively modestly. Thus, further integration of new inputs that give rise to the expansion of RFs and the pruning of non-preferred inputs that results in the sharpening of tuning may balance each other out such that response amplitudes are kept relatively stable post eye-opening. One possible explanation for the relatively stable response amplitudes in LM neurons post DR is that these two opposing events of integration and pruning are either unaffected by DR or affected to a similar degree, resulting in LM being seemingly resistant to DR. Future studies can reveal how single cell level RF properties in HVAs are affected by DR[41].

Implications for visual deficiency and disorders

The delayed development and sensitivity to dark rearing of dorsal stream HVAs suggest that these areas are particularly vulnerable to postnatal insults and developmental disorders of activity-dependent circuit refinement. Recovery of higher visual processing following early blindness is often incomplete in humans[42–44]. Furthermore, deficits of activity-dependent circuit refinement have been implicated in neurodevelopmental disorders including Fragile X syndrome and autism[45]. Accordingly, sensory processing deficits have been added to the diagnostic criteria for autism spectrum disorder in DSM-5 (ref. [46]). In particular, neurodevelopmental disorders are often accompanied by deficits in higher order visual processing. For example, in Fragile X syndrome, global motion perception attributed to dorsal stream function is impaired whereas acuity and global form recognition are normal[47]. Understanding the mechanisms for postnatal visual development as well as interrogating the V1 and HVA circuit deficits in the mouse models of these disorders would provide insights into the pathophysiology of these diseases. Our findings paint a complex picture, in which the two functionally discernible streams of visual pathway utilize distinct mechanisms for circuit development. Thus, therapeutic interventions towards circuit aberrations would likely require stream specific approaches.

METHODS

Animals and husbandry

All procedures involving living animals were carried out in accordance with the guidelines and regulations of the US Department of Health and Human Services and approved by the Institutional Animal Care and Use Committee at University of North Carolina. C57Bl/6 mice and GCaMP6s expressing transgenic mice (Allen Institute like Ai96 crossed with Emx1-Cre line, Jackson Labs stock #005628) of both sexes (Taconic) were housed under 12hr/12r dark light reverse cycle with ad libitum access to food and water. A subset of mice was reared in complete darkness from E14 to P40 ± 1 after which randomly selected some were immediately used and the remainder were further reared in the light until P65 ± 1. Infrared night vision goggles were used when servicing the mouse cages during dark rearing. Although it was impossible to completely blind experimenters during data gathering (e.g., younger mice are smaller), all subsequent quantification and analysis was performed blind to age and rearing conditions.

Randomization

For the developmental experiments, littermates within each litter were randomly assigned a different postnatal day for imaging. For DR experiments, littermates were randomly separated into dark-rearing until P65 vs. re-exposure to light from P45 through P65 groups.

Surgery

For acute imaging studies of developing mice, P13–18 pups were deeply anesthetized using isoflurane (5% for induction, 1–2% for surgery) augmented with chlorprothixene (2.5 mg/kg body weight, i.p.) as sedative. Physically-activated heat packs (SpaceGel, Braintree Scientific) were used to maintain the body temperature during surgery. The scalp overlaying

right visual cortex was removed, and a custom head-fixing imaging chamber with 5-mm diameter opening was mounted to the skull with cyanoacrylate-based glue (Oasis Medical) and dental acrylic (Lang Dental). Mice were mounted on a holder via the chamber, which was filled with a physiological saline containing (in mM) 150 NaCl, 2.5 KCl, 10 HEPES, 2 $CaCl_2$ and 1 $MgCl_2$. All imaging for the juvenile pups (≤ P18) was performed transcranially. For acute imaging of mice aged ≥ P40, the surgery proceeded as detailed above followed by a 4-mm diameter craniotomy over visual cortex.

For chronic repeated imaging of developing animals, P19 mice were anesthetized using isoflurane (5% for induction, 1 – 2.0% for surgery) augmented with acepromazine (0 – 0.4 mg/kg body weight, i.p.). A craniotomy was performed and sealed with a circular glass coverslip. Carprofen (4.4 mg/kg body weight, s.c.) was administered postoperatively to all mice that underwent recovery surgeries before returning to the home cage. The mice were imaged repeatedly every 4 days from P20 – P40.

Viral injections

Adeno-associated virus particles packaged and titered by the Penn Vector Core (~10^{12} infectious units per ml; University of Pennsylvania, Philadelphia) were used to overexpress genetically encoded calcium indicator, GCaMP6s (AAV1.Syn.GCaMP6s.WPRE.SV40). A craniotomy was performed as in for chronic imaging preps, and ISOI was used to map primary visual cortex (V1) and higher visual areas (HVAs) for targeted injections. In some experiments, ISOI was performed transcranially, and targeted burr holes were used for virus injections, in which case a craniotomy and optical window installation were carried out 4–6 weeks post injection. Viral particles were injected (100 – 250 nL per site) with a pulled glass capillary micropipette using a Nanoliter 2010 controlled by a microprocessor, Micro4 (World Precision Instruments) at 10 – 20 nL per minute. The glass pipette was left in place for 10 min before retracting to avoid backflushing of the injected solution. The cranial window was then sealed with a coverslip. Carprofen (4.4 mg per kg body weight, s.c.) was given postoperatively to all animals that underwent recovery surgeries before returning to their cage.

Intrinsic signal optical imaging (ISOI)

Custom instrumentation was adapted from Kalatsky and Stryker[29], similar to our prior work[26,28]. Two F-mount lenses with respective focal lengths of 135 and 50 mm (Nikon) formed a tandem lens macroscope, which was attached to Dalsa 1M30 CCD camera (Teledyne DALSA), which is a large well depth camera, which offers high signal-to-noise measurements in bright light conditions such as this. The macroscope configuration provided a 4.6 mm × 4.6 mm field of view (21.2 mm^2). Acquired images were binned 2 × 2 spatially, resulting in a final pixel size of 9.2 μm × 9.2 μm. The pial vasculature was illuminated through a green filter (550 ± 50 nm, Edmund Optics) and the vasculature map was captured through a second green filter (560 ± 5 nm). From the pial surface, the macroscope was then focused down 600 μm where intrinsic signals were illuminated with halogen light (Asahi Spectra) delivered via light guides and focusing probes (Oriel) through a red filter (700 ± 38 nm, Chroma). Reflected light was captured through a second red filter (700 ± 5 nm, Edmund Optics) at the rate of 30 frames per second with custom-made image

acquisition software (adapted from code kindly provided by D. Ferster, Northwestern University; to obtain this code contact either corresponding author). At 700 nm there is a large change in the absorption coefficient between oxyhemoglobin and deoxyhemoglobin, and thus this contributes to the intrinsic signal measured in these experiments. Mice were headfixed 20 cm from a flat 60 cm × 34 cm (width × height) monitor which was tilted towards the mouse 17.5° from vertical with their head angled to their right to cover the visual field (110° by 75°) of the contralateral eye. A light anesthetic plane was maintained with 0.5% isoflurane during imaging, augmented with either chlorprothixene (2.5 mg/kg body weight, i.p.) or acepromazine (0.4 – 3.0 mg/kg body weight, i.p., the lower end of this range was used P20 mice), and the body temperature was kept at 37°C using feedback-controlled electric heat pad systems (custom-built or FHC). Illumination stability was monitored by regular examination of individual pixel time courses to prevent this potential cause of imaging artifacts. In the case of unstable illumination, the imaging run was restarted. Mice were closely monitored for anesthetic depth as well. Increasing anesthetic depth decreases the signal strength, and complete wakefulness can cause imaging artifacts. These imaging artifacts appear to arise from large variations in cortical activity and blood vessel dilations and contractions that are uncorrelated with the stimulus, yet contain spectral strength that degrades the retinotopic map quality.

Visual stimuli

A drifting white bar on a black background (elevation and azimuth direction; 3° thick), drifting vertical grating patches (50° diameter, 2 cycles/s, 0.04 cycle/°), moving dots with 0 or 30% direction coherence, and a small square stimuli (10° × 10°) with drifting gratings of rapidly cycling through four directions (2 cycles/s, 0.04 cycle/°, 0.5 s per direction) were produced and presented using MATLAB and the Psychophysics Toolbox[48,49]. A corrective distortion was applied to all the visual stimuli except for moving dot kinematograms using a custom 3D model based MATLAB code in order to compensate for the flatness of the monitor[18] (code is available online, http://labrigger.com/blog/2012/03/06/mouse-visual-stim/). Grating patch and moving dot kinematogram stimuli were restricted to a central 50° region of the monocular visual hemifield, for two reasons: (1) to ensure activation of medial and lateral HVAs[23], and (2) to limit activation at the visual meridians that form the borders between cortical visual areas. Together, this is intended to minimize the influence of small expert-to-expert variations in the hand-drawn borders between HVAs based on retinotopy. Drifting motions occurred periodically for 50 repetitions at the last two seconds of an eight-second period (the small square stimulus was displayed for 250 repetitions). The image acquisition software employed fast Fourier transfer analyses of each pixel column to identify stimuli-evoked signals at this frequency and generated maps of response magnitude and phase at 0.125 Hz.

During two-photon calcium imaging, the visual stimulus LCD screen was shrouded with a cone up to the eye of the mouse to prevent contamination of the imaging pathway with light from the visual stimulus. The visual stimulus extended from +20 – +124° in azimuth and from −10 – +42° in elevation. Stimulus frames (128 × 128 pixels) were smoothly interpolated so that 1 stimulus frame pixel was equivalent to $0.72°^2$ in visual space.

For measuring orientation tuning, stimulus parameters were similar to a prior report[50]. Drifting square wave gratings (12 different directions, at 0.04 and 0.32 cycles/°, 2 Hz) were presented for 2 seconds at a time, with 2 seconds of grey screen (to maintain mean luminance) between grating presentations. For receptive field mapping, stimulus parameters were similar to a prior report[33], using a different random number generator seed for the stimulus generation algorithm. Sparse-noise visual stimuli consisted of black and white dots on a gray background. Dots ranged in size from 1.3–8.0° in diameter. Adjacent frames had no overlap in dot locations so that all pixel transitions were to or from gray, never from black to white or vice versa. Between 4,000 and 6,000 stimulus frames were used in each experiment. Total mapping time was 30–45 min.

Two-photon (2p) microscopy imaging

Ca^{2+} transients reported by GCaMP6s were imaged over 6 weeks post AAV injection (ISOI/2p calibration experiments) or at two developmental time points, P20 and P36, in GCaMP6s expressing transgenic mice, using a custom-built two-photon microscope using galvanometer-based scan mirrors (6mm diameter, Cambridge Technologies) with a 16 x magnification and 0.8 numerical aperture water immersion objective (Nikon) and a large aperture collection pathway with GaAsP photomultiplier tubes (Hamamatsu). Frame scans (1 frame/s or 15.6 frames/s) were acquired using ScanImage[51].

ISOI image analysis

Retinotopic maps were used to locate V1 and HVAs. Borders between these areas were drawn at the meridian of elevation and azimuth retinotopy. Magnitude response maps were also consulted for reconfirmation. ImageJ software (Fiji distribution[52]) was used to quantify response amplitudes at each region of interest (ROI). To exclude from analysis portions of cortex in the magnitude maps that did not significantly respond to the stimulus, a background magnitude value was determined and used as a threshold, called “background threshold”. For each image, the background threshold was determined on a 5×5 Gaussian-filtered image. Measurements were made for each ROI, from which the background threshold values were subtracted. Quantifications from this approach were highly reproducible between experts (Supplementary Fig. 1). For PCA analysis, 22-dimensional vectors were constructed (each mouse is one dimension) for each HVA. These 22-dimensional vectors were expressed as a linear combination of two principle components and plotted. Dorsal and ventral stream areas separated in the sign of the eigenvalue for the second principle component, for both responses to gratings and kinematograms (Component 2; Fig. 1i,j).

2p image analysis

Regions of interest (neuron locations in the image data) were identified using a semi-automated method. After spatiotemporal Gaussian filtering, the kurtosis of each pixel’s time course was computed. This creates a 2D map with contrast at neuron borders. This 2D map was binarized with a locally adaptive threshold, and potential regions of interest were automatically identified. Then, all data were examined manually to exclude artifacts and misidentified regions.

To ensure exclusion of low fidelity data, only neurons that exhibited at some point in the data set at least one event that exceeded 60% delta F/F were subjected to detailed analysis of tuning. For a neuron to be classified as tuned to oriented gratings, it had to respond to one of the grating types (direction and spatial frequency) on at least two of six trials[32]. For that metric, a "response" was an increase in fluorescence signal in excess of three standard deviations of the noise floor (measured during grey screen presentation). An ANOVA was performed to detect significantly tuned neurons for subsequent analysis. Responses from orientation tuned cells were averaged over trials and fit with a Gaussian function to extract OSI measurements as before[53].

Analysis of RF mapping was performed similar to a prior report[33]. Briefly, fluorescence time courses were deconvolved into estimated spike rates. Reverse correlation between estimate spike rates and sparse noise visual stimuli yielded separate maps of ON and OFF RF subregions. These raw subregions were z-scored and filtered. The resulting maps were thresholded (± 4 z-score) to obtain binarized maps that were analyzed to detect shared subregions[33]. To obtain measurements of subregion sizes, the binarized maps were used directly for area measurements; mean radius and long and short axes measurements were taken from elliptical fits of the binarized maps.

Statistical analysis

All quantifications were carried out blind to age and, in the dark rearing experiments, experimental conditions. In acute experiments, pups from individual litters were used for multiple time points. One mouse used for calcium imaging (identification code #67) was imaged at P20, but by P36 the window was no longer transparent enough for imaging. An additional mouse (identification code #68) was incorporated to make up for the loss of the one mouse. Custom software for Igor Pro (Wavemetrics) and MATLAB (MathWorks) were used to compute Pearson's *R*, two-way t-tests, and non-parametric rank-sum tests. Some *P*-values were computed to be extremely small (e.g., $< 10^{-200}$), however, it is difficult to assign meaning to such small values, so we chose to express *P*-values that are less than 0.0001 as that bound rather than their actual calculated value. JMP, Version 10.0.1 (SAS Institute) was used to compute ANOVA and Tukey-Kramer HSD, and to perform the correlation and PCA analyses. For correlation and PCA analyses, cortical areas were not grouped a priori, with the exception of areas AM and PM which were analyzed as a single region because the meridian between them was not always clearly resolved in retinotopic maps from ISO imaging. No statistical methods were used to pre-determine sample sizes but our sample sizes are similar to those reported in previous publications[3,20]. Data distribution is shown in each figure and was assumed to be normal, but this was not formally tested. In all figures, error bars and error clouds (shaded regions) indicate S.E.M.

To examine whether the effect size of the DR is stronger in certain HVAs, we analyzed the data using repeated measures ANOVA with the condition, HVA, and their interaction in the model with repeated measures (repeated response in each HVA) with an unstructured covariance matrix. The reference level for condition is the magnitude of response at age P65. The reference level for HVAs is RL.

We fit the model:

$$Y=\beta_0+\beta_1\times 40control+\beta_2\times 40DR+\beta_3\times 65+\beta_4\times AL+\beta_5\times AM+\beta_6\times LI+\beta_7\times LM+\beta_8\times AL\times 40C+\beta_9\times AM\times 40C+\beta_{10}\times LI\times 40C+\beta_{11}\times LM\times 40C+\beta_{12}\times AL\times 40DR+\beta_{13}\times AM\times 40DR+\beta_{14}\times LI\times 40DR+\beta_{15}\times LM\times 40DR+\beta_{16}\times AL\times 65C+\beta_{17}\times AM\times 65C+\beta_{18}\times LI\times 65C+\beta_{19}\times LM\times 65C+e$$

(“AM” = AM/PM, “40DR” = P40 dark reared, “40C” = P40 control, “65” = P65 recovery, “65C” = P65 control)

	Difference:40C-40DR	
	Estimate	**p-value**
AL vs. LI	0.1590	0.3677
AL vs. LM	**0.2407**	**0.0319***
AL vs. RL	0.3460	0.0873
AM/PM vs. LI	0.4246	0.0540
AM/PM vs. LM	**0.5063**	**0.0110***
AM/PM vs. RL	**0.6116**	**0.0035***
RL vs. LI	−0.1870	0.4109
RL vs. LM	−0.1053	0.6391

To read the table, take the first line: AL vs. LI (40C-40DR). The difference between 40C and 40 DR is 0.1590 greater in the AL group compared to the LI group. This means that the dark rearing effect size was larger in AL group, but this result wasn’t significant ($P = 0.3677$). By contrast, for AL vs. LM, the estimate was 0.2407 with a *P*-value of 0.0319. Therefore, DR effect size was significantly larger in AL compared to LM.

Data availability

The data that support the findings of this study are available from either corresponding author upon request.

Code availability

The custom intrinsic signal optical imaging code used for this study is available upon request from either corresponding author. The custom code for applying corrective distortion to the visual stimuli is available online at: http://labrigger.com/blog/2012/03/06/mouse-visual-stim/. The code for analyzing the 2p imaging data is available upon request.

Supplementary Material

Refer to Web version on PubMed Central for supplementary material.

Acknowledgments

We are grateful to D. Ferster for generously providing software for intrinsic signal optical imaging, and to J. Stirman for customizing the software for these experiments. We thank B. Philpot, P. Manis and J. Stirman for

helpful discussion and comments on the manuscript, and C. Mazzone for early contributions to the project. I.T.S. was supported by a Helen Lyng White Fellowship. L.B.S. was supported by a fellowship from the Howard Hughes Medical Institute/UNC-Chapel Hill Med into Grad program, and by the NIH (T32NS007431). This work was supported by a Career Development Award from the Human Frontier Science Program to S.L.S. (CDA 00063/2012), and grants from the Whitehall Foundation and the NIH (R01EY024294, R01NS091335) (S.L.S.).

References

1. Wang Q, Burkhalter A. Area map of mouse visual cortex. J Comp Neurol. 2007; 502:339–57. [PubMed: 17366604]
2. Wang Q, Gao E, Burkhalter A. Gateways of ventral and dorsal streams in mouse visual cortex. J Neurosci. 2011; 31:1905–18. [PubMed: 21289200]
3. Wang Q, Sporns O, Burkhalter A. Network analysis of corticocortical connections reveals ventral and dorsal processing streams in mouse visual cortex. J Neurosci. 2012; 32:4386–99. [PubMed: 22457489]
4. Liu YJ, et al. Tracing inputs to inhibitory or excitatory neurons of mouse and cat visual cortex with a targeted rabies virus. Curr Biol. 2013; 23:1746–55. [PubMed: 23993841]
5. Coogan TA, Burkhalter A. Hierarchical organization of areas in rat visual cortex. J Neurosci. 1993; 13:3749–72. [PubMed: 7690066]
6. Montero VM. Retinotopy of cortical connections between the striate cortex and extrastriate visual areas in the rat. Exp Brain Res. 1993; 94:1–15. [PubMed: 8335065]
7. Mishkin M, Ungerleider LG. Contribution of striate inputs to the visuospatial functions of parieto-preoccipital cortex in monkeys. Behav Brain Res. 1982; 6:57–77. [PubMed: 7126325]
8. Mishkin, M., Ungerleider, LG. Two cortical visual systems. In: Ingle, DJea, editor. Analysis of Visual Behavior. MIT Press; 1982. p. 549-586.
9. Newsome WT, Pare EB. A selective impairment of motion perception following lesions of the middle temporal visual area (MT). J Neurosci. 1988; 8:2201–11. [PubMed: 3385495]
10. Barton JJ. Disorders of higher visual processing. Handb Clin Neurol. 2011; 102:223–61. [PubMed: 21601069]
11. Wang Q, Burkhalter A. Stream-related preferences of inputs to the superior colliculus from areas of dorsal and ventral streams of mouse visual cortex. J Neurosci. 2013; 33:1696–705. [PubMed: 23345242]
12. De Pasquale R, Sherman SM. A modulatory effect of the feedback from higher visual areas to V1 in the mouse. J Neurophysiol. 2013; 109:2618–31. [PubMed: 23446698]
13. De Pasquale R, Sherman SM. Modulatory effects of metabotropic glutamate receptors on local cortical circuits. J Neurosci. 2012; 32:7364–72. [PubMed: 22623682]
14. De Pasquale R, Sherman SM. Synaptic properties of corticocortical connections between the primary and secondary visual cortical areas in the mouse. J Neurosci. 2011; 31:16494–506. [PubMed: 22090476]
15. Ji W, et al. Modularity in the Organization of Mouse Primary Visual Cortex. Neuron. 2015; 87:632–43. [PubMed: 26247867]
16. Sherman SM. The function of metabotropic glutamate receptors in thalamus and cortex. Neuroscientist. 2014; 20:136–49. [PubMed: 23459618]
17. Sherman SM. Thalamus plays a central role in ongoing cortical functioning. Nat Neurosci. 2016; 16:533–41.
18. Marshel JH, Garrett ME, Nauhaus I, Callaway EM. Functional specialization of seven mouse visual cortical areas. Neuron. 2011; 72:1040–54. [PubMed: 22196338]
19. Andermann ML, Kerlin AM, Roumis DK, Glickfeld LL, Reid RC. Functional specialization of mouse higher visual cortical areas. Neuron. 2011; 72:1025–39. [PubMed: 22196337]
20. Glickfeld LL, Andermann ML, Bonin V, Reid RC. Cortico-cortical projections in mouse visual cortex are functionally target specific. Nat Neurosci. 2013; 16:219–26. [PubMed: 23292681]
21. Gao E, DeAngelis GC, Burkhalter AH. Specialized areas for shape and motion analysis in mouse visual cortex. Society for Neuroscience Annual Meeting. 2006; 32:641.6.

22. Juavinett AL, Callaway EM. Pattern and Component Motion Responses in Mouse Visual Cortical Areas. Curr Biol. 2015; 25:1759–64. [PubMed: 26073133]
23. Tohmi M, Takahashi K, Kubota Y, Hishida R, Shibuki K. Transcranial flavoprotein fluorescence imaging of mouse cortical activity and plasticity. J Neurochem. 2009; 109(Suppl 1):3–9. [PubMed: 19393002]
24. Garrett ME, Nauhaus I, Marshel JH, Callaway EM. Topography and areal organization of mouse visual cortex. J Neurosci. 2014; 34:12587–600. [PubMed: 25209296]
25. Pisauro MA, Dhruv NT, Carandini M, Benucci A. Fast hemodynamic responses in the visual cortex of the awake mouse. J Neurosci. 2013; 33:18343–51. [PubMed: 24227743]
26. Smith SL, Trachtenberg JT. The refinement of ipsilateral eye retinotopic maps is increased by removing the dominant contralateral eye in adult mice. PLoS One. 2010; 5:e9925. [PubMed: 20369001]
27. Zuo Y, Lin A, Chang P, Gan WB. Development of long-term dendritic spine stability in diverse regions of cerebral cortex. Neuron. 2005; 46:181–9. [PubMed: 15848798]
28. Smith SL, Trachtenberg JT. Experience-dependent binocular competition in the visual cortex begins at eye opening. Nat Neurosci. 2007; 10:370–5. [PubMed: 17293862]
29. Kalatsky VA, Stryker MP. New paradigm for optical imaging: temporally encoded maps of intrinsic signal. Neuron. 2003; 38:529–45. [PubMed: 12765606]
30. Cang J, et al. Development of precise maps in visual cortex requires patterned spontaneous activity in the retina. Neuron. 2005; 48:797–809. [PubMed: 16337917]
31. Schuett S, Bonhoeffer T, Hubener M. Mapping retinotopic structure in mouse visual cortex with optical imaging. J Neurosci. 2002; 22:6549–59. [PubMed: 12151534]
32. Rochefort NL, et al. Development of direction selectivity in mouse cortical neurons. Neuron. 2011; 71:425–32. [PubMed: 21835340]
33. Smith SL, Hausser M. Parallel processing of visual space by neighboring neurons in mouse visual cortex. Nat Neurosci. 2010; 13:1144–9. [PubMed: 20711183]
34. Kremkow J, Jin J, Wang Y, Alonso JM. Principles underlying sensory map topography in primary visual cortex. Nature. 2016; 533:52–7. [PubMed: 27120164]
35. van den Boomen C, van der Smagt MJ, Kemner C. Keep your eyes on development: the behavioral and neurophysiological development of visual mechanisms underlying form processing. Front Psychiatry. 2012; 3:16. [PubMed: 22416236]
36. Ko H, et al. The emergence of functional microcircuits in visual cortex. Nature. 2013; 496:96–100. [PubMed: 23552948]
37. Braddick O, Atkinson J, Wattam-Bell J. Normal and anomalous development of visual motion processing: motion coherence and ‘dorsal-stream vulnerability’. Neuropsychologia. 2003; 41:1769–84. [PubMed: 14527540]
38. Spencer J, et al. Motion processing in autism: evidence for a dorsal stream deficiency. Neuroreport. 2000; 11:2765–7. [PubMed: 10976959]
39. Tohmi M, Meguro R, Tsukano H, Hishida R, Shibuki K. The extrageniculate visual pathway generates distinct response properties in the higher visual areas of mice. Curr Biol. 2014; 24:587–97. [PubMed: 24583013]
40. Hoy JL, Niell CM. Layer-specific refinement of visual cortex function after eye opening in the awake mouse. J Neurosci. 2015; 35:3370–83. [PubMed: 25716837]
41. Vorobyov V, Kwok JC, Fawcett JW, Sengpiel F. Effects of digesting chondroitin sulfate proteoglycans on plasticity in cat primary visual cortex. J Neurosci. 2013; 33:234–43. [PubMed: 23283337]
42. Ellemberg D, Lewis TL, Maurer D, Brar S, Brent HP. Better perception of global motion after monocular than after binocular deprivation. Vision Res. 2002; 42:169–79. [PubMed: 11809471]
43. Le Grand R, Mondloch CJ, Maurer D, Brent HP. Neuroperception. Early visual experience and face processing. Nature. 2001; 410:890. [PubMed: 11309606]
44. Le Grand R, Mondloch CJ, Maurer D, Brent HP. Expert face processing requires visual input to the right hemisphere during infancy. Nat Neurosci. 2003; 6:1108–12. [PubMed: 12958600]

45. Ebert DH, Greenberg ME. Activity-dependent neuronal signalling and autism spectrum disorder. Nature. 2013; 493:327–37. [PubMed: 23325215]
46. Association, A.P. Diagnostic and statistical manual of mental disorders. 5. American Psychiatric Publishing; Arlington, VA: 2013.
47. Kogan CS, et al. Differential impact of the FMR1 gene on visual processing in fragile X syndrome. Brain. 2004; 127:591–601. [PubMed: 14736752]
48. Brainard DH. The Psychophysics Toolbox. Spat Vis. 1997; 10:433–6. [PubMed: 9176952]
49. Pelli DG. The VideoToolbox software for visual psychophysics: transforming numbers into movies. Spat Vis. 1997; 10:437–42. [PubMed: 9176953]
50. Smith SL, Smith IT, Branco T, Hausser M. Dendritic spikes enhance stimulus selectivity in cortical neurons in vivo. Nature. 2013; 503:115–20. [PubMed: 24162850]
51. Pologruto TA, Sabatini BL, Svoboda K. ScanImage: flexible software for operating laser scanning microscopes. Biomed Eng Online. 2003; 2:13. [PubMed: 12801419]
52. Schindelin J, et al. Fiji: an open-source platform for biological-image analysis. Nat Methods. 2012; 9:676–82. [PubMed: 22743772]
53. Cottam JC, Smith SL, Hausser M. Target-specific effects of somatostatin-expressing interneurons on neocortical visual processing. J Neurosci. 2013; 33:19567–78. [PubMed: 24336721]

Summary

Vison is processed across multiple cortical areas that are organized into two subnetworks in primates. However, the generality of this organization and its development are unclear. Smith and colleagues present functional evidence for the analogous two subnetworks in mice, and map their differential developmental dynamics.

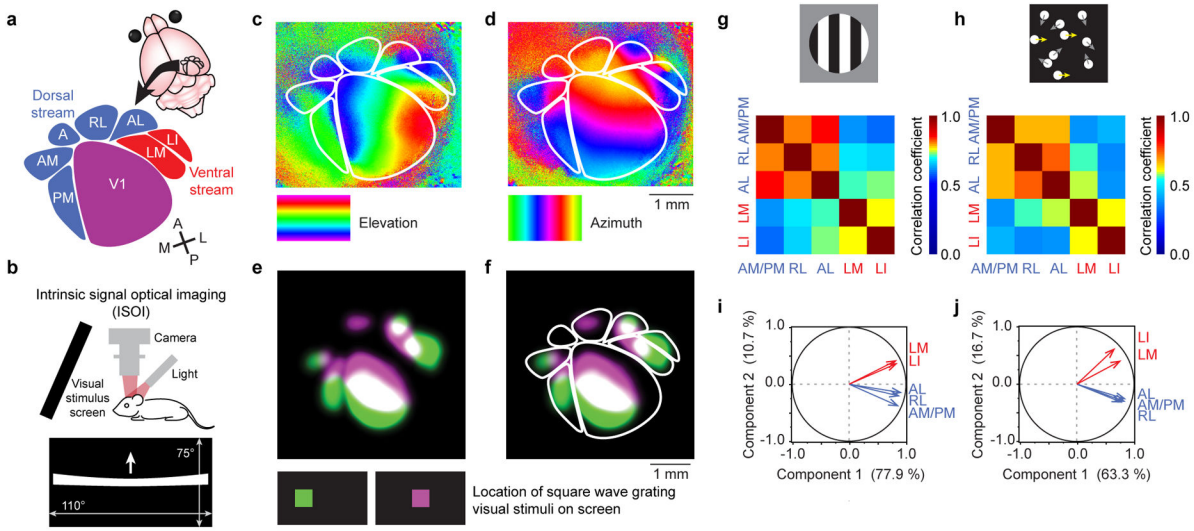

Figure 1. Mapping and functional grouping of putative dorsal and ventral stream higher visual areas (HVAs) in mice

(a) Schematic view of the cortical location of V1 and HVAs in the right hemisphere, assigned to putative dorsal and ventral streams following the work of Burkhalter, Wang, and colleagues[2,3]. (b) Intrinsic optical signals were measured as decreases in the reflectance of red (700 nm) light as cortical regions were activated, measured using a tandem lens macroscope and a CCD camera. The visual stimulus monitor was tilted towards the mouse, and covered 110° of horizontal, and 75° of vertical visual field. The mouse was centered in front of the monitor, with its nose pointed towards the right side, to maximize coverage of the left visual hemifield. To map retinotopy, a single white bar drifted across the screen (horizontal or vertical, warped to ensure isoelevation and isoazimuth activation patterns). (c) Elevation and (d) azimuth maps revealed the meridians of retinotopy that form the borders among visual cortical areas. Cortex is color-coded according to the location of the bar on the monitor at the time of the evoked visual response. The locations of HVAs were drawn based on these retinotopic maps for each mouse individually. Rigid templates were not used. (e) To further confirm the location of HVAs, gratings were displayed in small square apertures, and the resulting activation pattern was used to locate retinotopically active areas in V1 and HVAs. Two maps were generated, each with the aperture in a different azimuthal location on the monitor (color-coded green and violet). (f) The spatial relationship between the two evoked maps matched the predictions from the (c) elevation and (d) azimuth retinotopic maps. (g,h) Maps evoked by stimulation with gratings (g) or kinematograms (h) both exhibited responses that were significantly correlated among dorsal stream HVAs, and among ventral stream HVAs, but less correlated between the two streams. (i,j) Principal component analysis (22-dimensional vectors for $n = 22$ mice), carried out independently for maps from (i) gratings and (j) kinematograms, indicated that dorsal and ventral stream HVAs exhibit correlated variability. These analyses provide functional evidence that AL, RL, and AM/PM belong to one subnetwork, and LM and LI belong to another. Correlation values and statistics are shown in Supplementary Table 1.

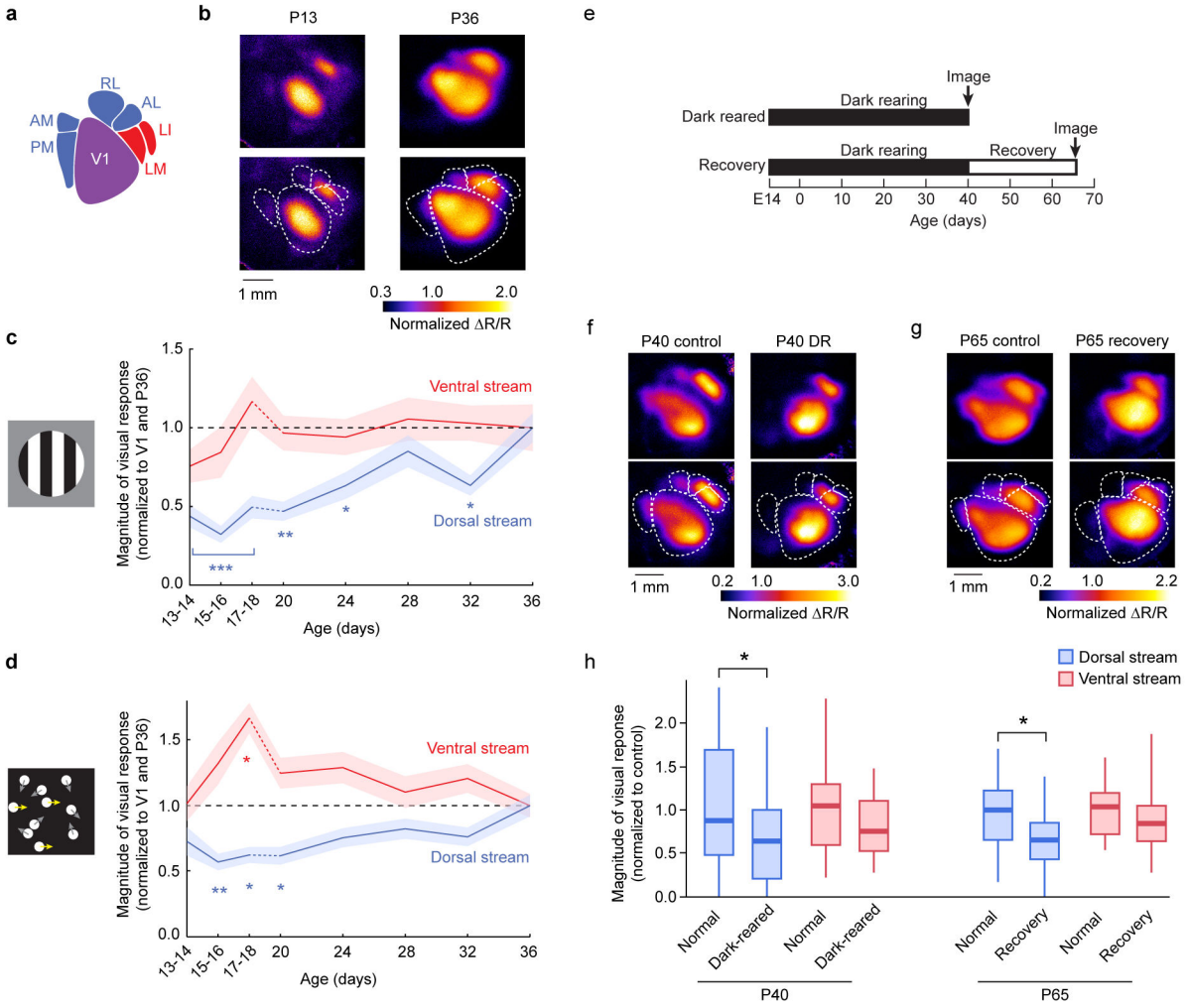

Figure 2. Functional responses in dorsal stream areas develop more slowly and are more dependent on experience than in ventral stream areas

(a) Responses in V1 and HVAs were measured (b) at ages P13 through P36. For P13–P18, data were taken from acute preparations (a single time point per mouse, 2 consecutive ages pooled as shown), and for P20–P36 as chronic preparations (multiple time points per mouse). Retinotopic maps defined the locations of V1 and HVAs within each mouse and time point. (c) Responses to drifting gratings rapidly matured in ventral stream HVAs whereas visually evoked responses in dorsal stream HVAs were slower to develop. (d) Responses to random dot kinematograms in ventral stream HVAs were strong early after eye opening, but those in dorsal stream HVAs were weaker and grew more slowly in magnitude. (e) One set of mice (“Dark reared” or “DR”) were reared in complete darkness from E14 to P40, and compared to normally reared P40 mice. Another set of mice (“Recovery”) were also dark-reared to P40, but then were provided 25 days of normal light-dark cycle housing. These mice were compared to normally reared P65 mice. Multiple litters were used for each group. (f,g) Example maps show that evoked responses of dorsal stream HVAs in DR and Recovery mice were weak compared to control mice at the same ages. (h) In both dark reared and recovery mice, dorsal stream HVAs exhibited significantly weaker responses,

while ventral stream HVAs remained unaffected. *** indicates $P < 0.0001$ for each of the three time points; ** $P = 0.001$; * $P < 0.05$ (ANOVA followed by Tukey-Kramer HSD for panels c,d). Shaded regions in (c,d) indicate SEM. Each box plot in (h) indicates the median (thick line), the range of middle two quartiles (shaded boxes), and the full data range (whiskers).

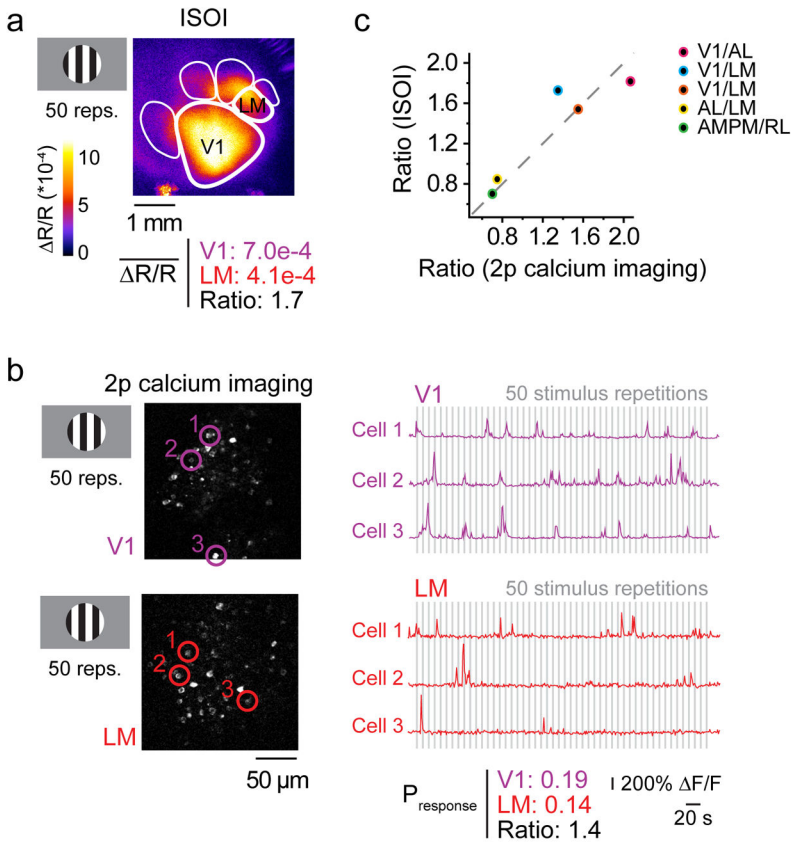

Figure 3. Visually evoked responses measured as ISOI signals correlate with action potential-associated calcium signals

To validate the quantitative measurements from ISOI signals, visually evoked cortical activity was measured in the same mice using both ISOI and 2-photon (2p) calcium imaging. (a) A square wave grating stimulus (drifting for 2 s, stationary for 6 s) evoked activity in V1 and HVAs, and the average change in reflectance ($\Delta R/R$) over 50 repetitions was recorded via ISOI. (b) Population activity, with single neuron resolution, was measured using 2p calcium imaging of neurons. Example images show V1 and LM neurons expressing GCaMP6s. The same visual stimulus was used. Example traces show responses from 6 neurons (circled and color coded in the images on the left) to 50 repetitions of the stimulus used to measure the average probability of response to the stimulus in V1 and LM (grey bars indicate the 2 seconds during which the grating drifted). (c) The ratios of responsiveness between two cortical areas were the same whether measured with ISOI or 2p calcium imaging ($n = 10$ cortical areas, 5 intra-mouse comparisons, 3 mice; Pearson's $R = 0.92$; $P = 0.027$). Data from panels (a) and (b) are represented by the blue data point. The other colored points represent different pairs of cortical areas as indicated in the inset. Thus, ISOI provides a faithful report of evoked activity in V1 and HVAs simultaneously.

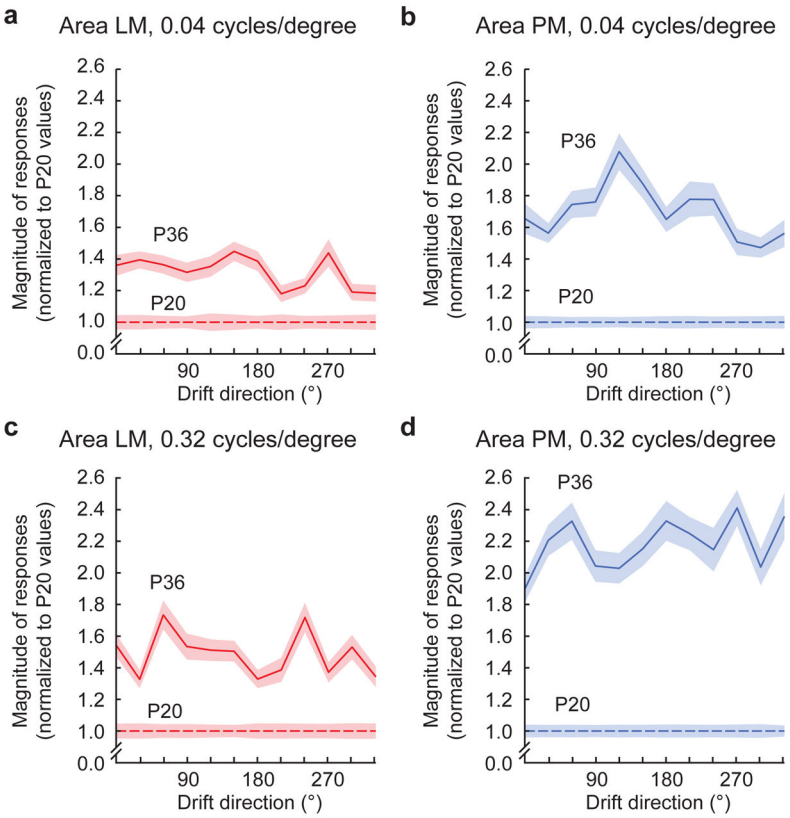

Figure 4. Response magnitude increases in areas PM and LM from P20 to P36 measure with 2p calcium imaging

(a) With 0.04 cycle/degree gratings, response magnitudes to oriented gratings in area LM increased from P20 to P36, (b) while a larger increase occurred for neurons in area PM. (c,d) With 0.32 cycle/degree gratings, response magnitudes increased for both LM and PM from P20 to P36. Again, the relative increase for area PM was larger than the increase for neurons in area LM. Shaded regions indicate SEM.

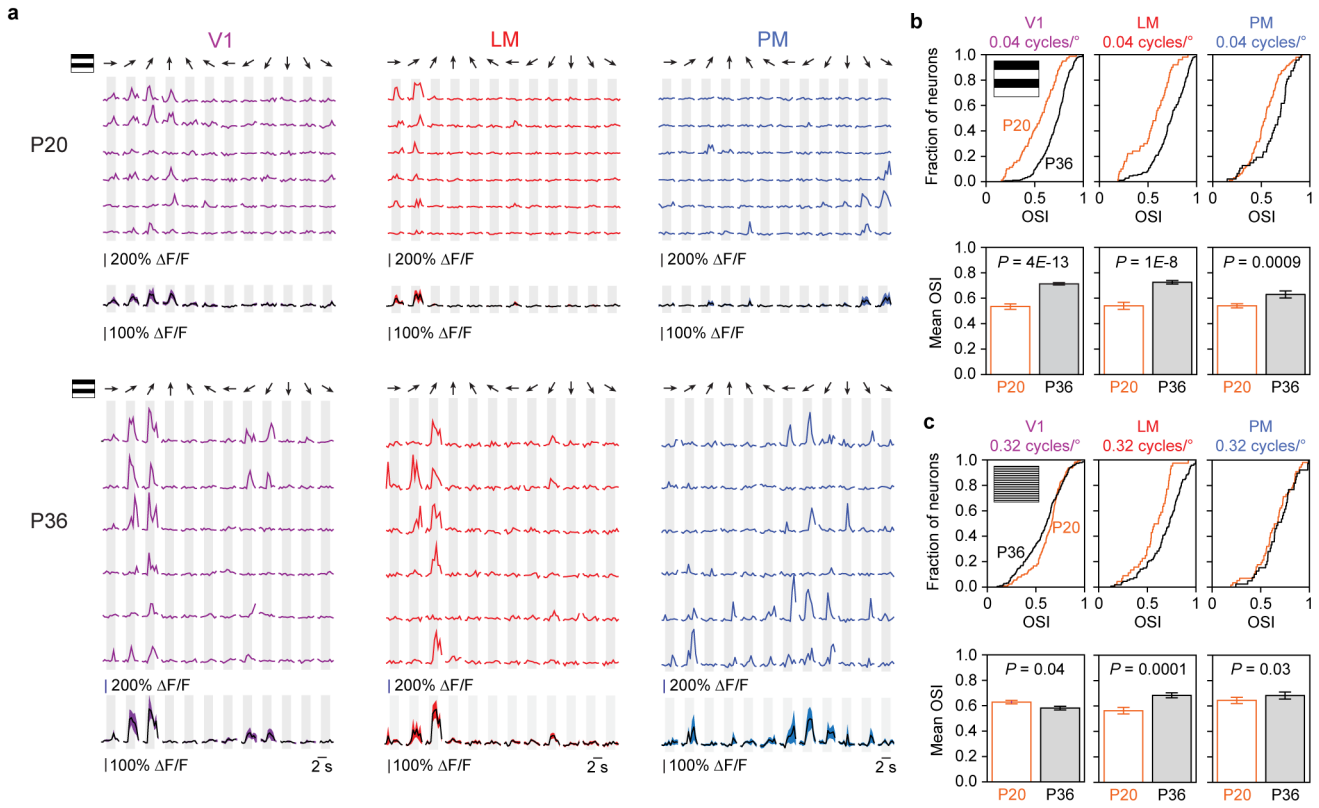

Figure 5. Orientation tuning changes in areas V1, LM, and PM from P20 to P36

(a) Data from six different example cells in areas V1, LM, and PM in P20 and P36 mice. Single sweeps (top) and mean +/− SEM (bottom) show orientation tuned responses (12 directions). (b) Population data for orientation tuning in areas V1, LM, and PM at P20 and P36 for 0.04 cycles/degree and (c) 0.32 cycles/degree gratings. Both cumulative histograms (top rows of b,c) and bar graphs (bottom rows of b,c; mean ± SEM) are shown for each data set.

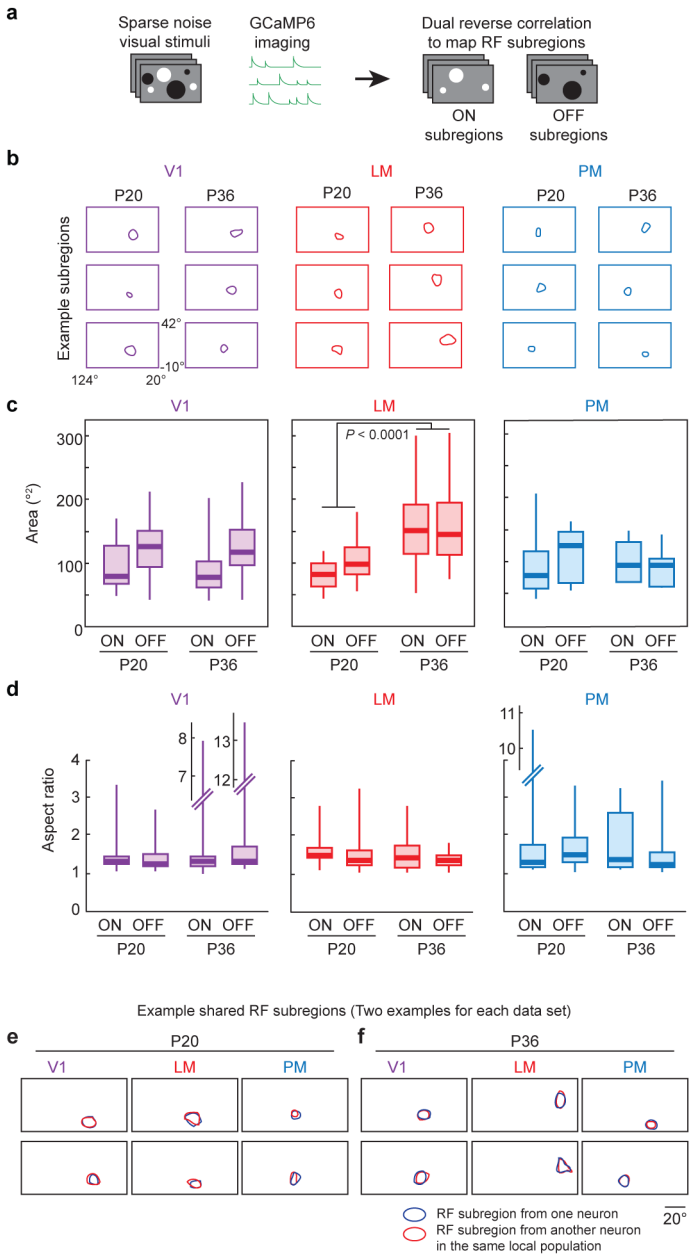

Figure 6. Receptive field subregion changes in areas V1, LM, and PM from P20 to P36

(a) RF subregions were mapped using sparse noise visual stimulation. Reverse correlation was used with the white and black dots separately to independently recover the ON and OFF RF subregions. (b) Example RF subregions for areas V1, LM, and PM at ages P20 and P36. (c) Both ON and OFF subregions increased in size in area LM between P20 and P36. Similar increases were not detected in areas V1 or PM. (d) Aspect ratios of RF subregions did not significantly change between P20 and P36. (e) Shared RF subregions were observed in areas V1, LM, and PM at both P20, and (f) P36. Each box plot in (c,d) indicates the

median (thick line), the range of the middle two quartiles (shaded boxes), and the full data range (whiskers).